arktos (2018) 4:21
https://doi.org/10.1007/s41063-018-0057-8

ORIGINAL ARTICLE

Improved Pleistocene sediment stratigraphy and paleoenvironmental implications for the western Arctic Ocean off the East Siberian and Chukchi margins

Michael Schreck[1,2] · Seung-Il Nam[2] · L. Polyak[3] · C. Vogt[4] · G.-S. Kong[5] · R. Stein[6] · J. Matthiessen[6] · F. Niessen[6]

Received: 25 January 2018 / Accepted: 22 June 2018

Abstract
Sediment cores from the East Siberian and Chukchi margins and adjacent basins are used to refine the upper Pleistocene stratigraphy and better constrain the timing of major glacial advances in the western Arctic Ocean. Cores have been analysed using high-resolution non-destructive physical properties (density, magnetic susceptibility and colour) and X-ray fluorescence elemental measurements (manganese and calcium contents). All analysed cores reveal a spatially coherent stratigraphic pattern that enables robust correlations from the East Siberian margin to the Mendeleev and Northwind Ridges, thus highlighting the potential of such multiproxy approach for improving stratigraphic framework. The distribution of sedimentary units resulting from core correlation indicates decreasing sedimentation rates by more than one order of magnitude from the East Siberian margin east- and northwards, reflecting an increased distance from the main sediment sources, increasing sea-ice cover, and longer residence times in the Beaufort Gyre circulation. The stratigraphy presented, consistent with existing geophysical data, indicates the most recent major glacial advance from the East Siberian margin with ice grounding at water depth > 800 m during estimated Marine Isotope Stages 4/3, roughly contemporaneous with the Middle Weichselian glaciation in northern Eurasia. Earlier glacial events are potentially indicated by glaciogenic units in cores away from the margin, where they are not overprinted by a younger ice advance. Sediment thickness increase towards the Siberian margin also suggests the possibility of a limited MIS 2 glaciation, although no direct evidence for such an ice sheet has been found thus far.

Keywords Arctic Ocean · Non-destructive measurements · Stratigraphy · Middle and Late Weichselian glaciation

Introduction

Insufficiently constrained sediment stratigraphy continues to be a major impediment for comprehending climatic and oceanographic development of the Arctic Ocean. Its nearly land-locked, circumpolar position and a profound role of

Electronic supplementary material The online version of this article (https://doi.org/10.1007/s41063-018-0057-8) contains supplementary material, which is available to authorized users.

✉ Michael Schreck
Michael.Schreck@uit.no

✉ Seung-Il Nam
sinam@kopri.re.kr

[1] Department of Geosciences, UiT The Arctic University of Norway, P.O. Box 6050, Langnes, 9037 Tromsø, Norway

[2] Division of Polar Paleoenvironment, Korea Polar Research Institute, 26 Songdomirae-ro, Yeonsu-gu, Incheon 21990, Republic of Korea

[3] Byrd Polar and Climate Research Center, The Ohio State University, 1090 Carmack Road, Columbus, OH 43210, USA

[4] Fachbereich Geowissenschaften, University Bremen, Klagenfurter Strasse 2-4, 28359 Bremen, Germany

[5] Korea Institute for Geoscience and Mineral Resources, 124 Gwahak-ro, Yuseong-gu, Daejeon 305-350, Republic of Korea

[6] Alfred Wegener Institute, Helmholtz Centre for Polar and Marine Research, Am Alten Hafen 26, 27568 Bremerhaven, Germany

Published online: 05 July 2018

wide and shallow continental margins complicates establishing a chronostratigraphic framework for Arctic Ocean sediments due to adverse effects of sea-ice cover, sea-level fluctuations, and extensive glaciations. In addition to widely acknowledged North American and Barents–Kara ice sheets, recent seafloor mapping in the western Arctic Ocean revealed recurrent grounding of voluminous ice-sheets and/or ice-shelves at the East Siberian and Chukchi margins and adjacent submarine ridges [1–8]. Constrains on the temporal occurrence and spatial extent of marine-based ice sheets in the Amerasian Arctic are critical for understanding the history of their build-up and decay, but attendant age models and stratigraphic correlations are still in an early stage of development.

To provide insights into Pleistocene stratigraphy of the western Arctic Ocean, we use a set of new, high-quality sediment cores recovered by RV Araon and RV Polarstern from the major ridges and basins adjacent to the East Siberian and Chukchi margins. Based on continuous, non-destructive, high-resolution down-core measurements of sediment colour, physical properties (bulk density and magnetic susceptibility), and X-ray fluorescence, we propose a stratigraphic correlation of sediment cores across this part of the western Arctic Ocean. This correlation provides improved stratigraphic constraints for late Pleistocene glaciations in the eastern Siberia and Beringian region and helps to characterize related depositional environments.

Geographic and stratigraphic background

The Amerasian Basin generally coincides with the western Arctic and is bounded by the Lomonosov Ridge, eastern Siberia, Alaska and the Canadian Arctic Archipelago (Fig. 1). Its present day surface water circulation is dominated by the wind-driven anticyclonic Beaufort Gyre. The basin is characterized by a restricted hydrographic exchange with adjacent regions due to limited deep-water exchange across the Lomonosov Ridge, the shallow Bering Strait and the Canadian Arctic Archipelago, and the residue times of water masses within the Beaufort Gyre. This isolation complicates comparisons with other oceans, including the Eurasian Basin of the Arctic Ocean, and thus hinders stratigraphic and paleoclimatic studies, in particular beyond the reach of AMS ^{14}C dating [9].

Early studies of Arctic Ocean sediment cores primarily relied on magnetostratigraphic interpretations. The correlation of inclination changes to magnetic reversals resulted in age models suggesting very low sedimentation rates in the order of factions of mm kyr^{-1} (e.g. [10] and references therein). These early age models and derived sedimentation rates, however, partly displayed discrepancies when compared to AMS ^{14}C ages [11] and/or the lithological placement of glacial–interglacial cycles (e.g. [9, 12, 13]). Indeed, multiple studies in the last two decades have suggested that inclination changes in Arctic Ocean sediment cores may represent magnetic excursions instead of full reversals [14–19]. This inference resulted in estimation of significantly higher sedimentation rates (up to a few cm kyr^{-1} in some areas), a pattern that is now widely accepted (e.g. [9, 10, 13]). However, paleomagnetic interpretations still remain vague as origin of inclination swings in Arctic Ocean sediments is not entirely resolved, and the inclination changes might even be lithologically (diagenetically) rather than geomagnetically controlled [20, 21].

The establishment of age–depth relationships in Arctic Ocean sediment cores is additionally complicated by the strong dissolution of calcareous microfossils (e.g. [22] and references therein), which restricts their application for biostratigraphy and stable isotope stratigraphy. In addition, ecological factors (e.g. sea-ice cover) and/or dilution by terrigenous material may influence their temporal distribution (see Ref. [23] and references therein). Stable isotope stratigraphy is complicated by surface hydrological processes (riverine inputs, sea-ice formation and melting, brine rejection), strongly influencing the nearly landlocked Arctic Ocean, in particular the hydrographically isolated Amerasian Basin, on timescales from seasonal to glacial–interglacial cycles [12, 19, 24, 25]. While attempts have been made to link Arctic Middle to Late Quaternary biostratigraphy to the standard MIS chronology [22], core-to-core correlation still mainly relies on lithostratigraphy (see Ref. [13]).

For the Amerasian Basin, a widely accepted lithostratigraphy has been established in early studies based on sedimentological characterization of numerous, relatively short sediment cores [26]. This lithostratigraphy was primarily based on the content of sand-sized material and a common occurrence of so-called pink–white (PW) and white (W) layers shown to be useful for core correlation across most of the western Arctic Ocean (e.g. Refs. [13, 26–28]). Although the number and extent of these layers may vary between cores depending on location (and thus sedimentation rates), three prominent layers, labelled W3, PW2 and PW1 in order of their down-core occurrence, have been identified in most cores [9, 12, 13, 22, 26]. Based on more detailed studies, these marker horizons represent diamictons characterized by dolomitic ice (iceberg)-rafted debris [12, 13, 27, 29–31]. A common source for dolomite in Arctic Ocean sediments is erosion of Palaeozoic rocks cropping out in the Canadian Arctic Archipelago (e.g. [29]). The North American origin of these layers has recently been confirmed by lead and neodymium isotope studies of their detrital components in Pleistocene sediments from the Mendeleev Ridge [32]. The formation of pinkish-white layers has been thus related to the disintegration of an extended Laurentide Ice Sheet and

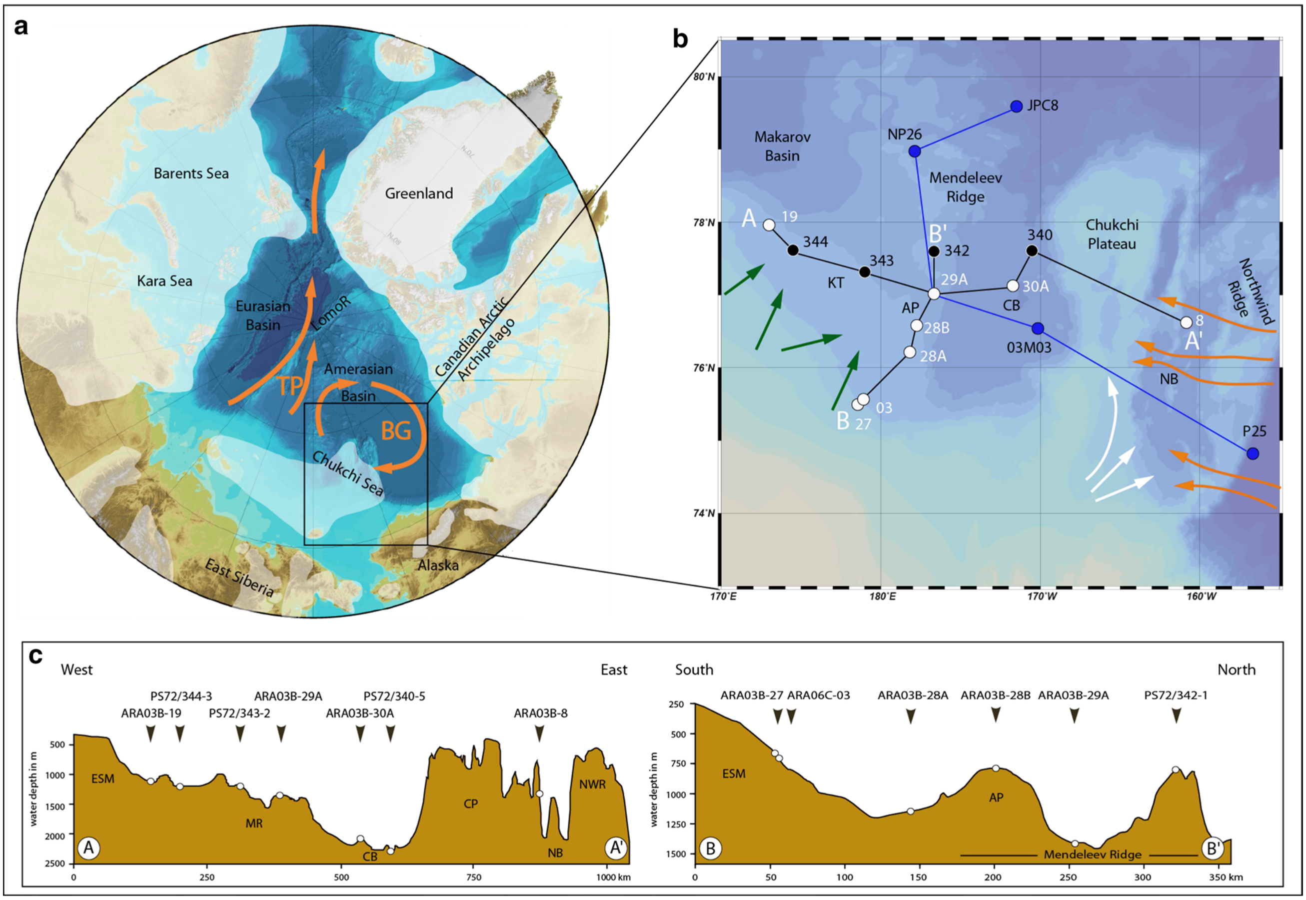

Fig. 1 **a** Overview map of the Arctic Ocean. Arrows (yellow) show modern surface circulation (modified after Ref. [55]). Bathymetry is based on the International Bathymetric Chart of the Arctic Ocean [66]. White overlays show the maximum Quaternary ice-sheet extents (from Refs. [5, 67]). Rectangle marks the study area. **b** Map of the study area with location of cores used. White dots = ARA03B and ARA06C cores (2012, 2015); black dots = PS72 cores (2008); blue dots = ^{14}C/AAR-dated cores from prior studies: NP26 = composite of NP26-5 and NP26-32 [12], JPC8 = HLY0503-8JPC [34], 03M03 [39], P25 = 92AR-P25 [40]. Black line indicates position of transects A (A–A′) and B (B–B′). Blue line indicates position of transect shown in Fig. 2. Arrows illustrate inferred ice flow directions of different provenance (from Refs. [5, 6, 66]): orange = Laurentide, green = East Siberian, white = Chukchi. *AP* Arliss Plateau, *CB* Chukchi Basin, *NB* Northwind Basin, *KT* Kucherov Terrace. **c** Bathymetric profiles and core location along transects A and B. *ESM* East Siberian margin

subsequent transport by icebergs during glacial terminations [12, 13, 27, 31–33].

Variations in lithology and occurrence of stratigraphic marker beds as recorded by physical property measurements have also been proven a useful tool for core correlations [28]. However, long-distance (inter-basin) correlations are complicated by differences in sediment composition in different regions of the Arctic Ocean, and therefore, require using multiple proxies developed by litho-, chemo-, and biostratigraphic studies.

Apart from the lithostratigraphic scheme of Clark et al. [26], core correlation in the western Arctic Ocean is primarily based on cyclic occurrence of dark brown intervals intercalated with lighter coloured, yellowish to greyish sediments. These conspicuous brown units are ubiquitous in the western Arctic Ocean (e.g. [12, 13, 26]) and are generally characterized by minima in sediment lightness (L^*) and wet-bulk density, low to moderate amounts of ice-rafted debris (IRD), high numbers of faunal remnants, and increased contents of manganese (oxyhydr)oxides, which provide the brown colour (e.g. [9, 13, 34–36]). The synchronicity of enhanced bioturbation and elevated microfossil abundance suggests that the Mn-rich brown units correspond to interglacial and/or major interstadial intervals. Conversely, the yellowish to greyish sediments, almost unfossiliferous and largely fine grained, are thought to present glacial intervals, when the main Mn sources (riverine input and coastal erosion) were largely reduced as continental ice blocked or redirected the Arctic rivers, and large parts of the shelf were exposed, thus leading to deposition of sediments depleted in Mn [35, 36]. The resulting cyclic pattern of Mn in Arctic Ocean sediments is, therefore, thought to follow major glacial/interglacial changes [34], and the brown/grey units have been shown useful for lithostratigraphic correlations, especially in the Amerasian Basin (e.g. [9, 13, 37]). However, secondary controls on down-core Mn variations, such as heterogeneity of sources, distribution processes, and diagenetic overprint, may put constrains on long-distance correlations using Mn cycles alone [36, 38]. Overall, existing results show that multiple proxies are needed for a reliable lithostratigraphy, including independent physical, chemical, and/or biological indicators.

Here we focus on comparing the down-core distribution of Mn and Ca, along with sediment colour and physical properties as a time-saving, multi-proxy correlation approach, shown to be efficient by prior studies (e.g. [9, 13, 28]). Correlation with earlier developed records, notably cores NP26 [12], HLY0503-08JPC [34], 03M03 [39] and 92AR-P25 [40], is used for better age control and a more comprehensive regional lithostratigraphic characterization.

Materials and methods

Sediment cores

Cores reported in this study (Fig. 1; Table 1) have been recovered during the 2008 expedition of the RV Polarstern (PS72) [13, 41], and more recently during the RV Araon expeditions ARA03B (2012, Ref. [42]) and ARA06C (2015). All coring positions have been chosen using detailed multi-beam bathymetric mapping and sub-bottom acoustic profiling.

Lithostratigraphy of the Polarstern cores has been previously described and provided with a tentative age model [13]. The core correlation and the initial age model are based on the content of sand-sized material, distinct brown units and prominent pink–white layers. Using a combination of continuously measured sediment colour, physical properties (density and magnetic susceptibility), and element count ratios (manganese and calcium), we re-evaluate the correlation of the Polarstern cores and extend their spatial coverage by integrating recently recovered Araon cores (Fig. 1). The cores selected for this study are arranged in two transects: (A) from the Kucherov Terrace at the East Siberian continental margin in the west to the Northwind Basin in the east, and (B) stretching longitudinally along the Mendeleev Ridge from the East Siberian margin at ~74°N to ~78°N.

To establish age control for cores under study, they have been correlated to sediment records with established age models including ^{14}C ages supplemented by ^{14}C-calibrated amino acid racemization (AAR) data (Fig. 2, Supplementary Table 1). Correlation is exemplified by core ARA03B-29A that ties transects A and B. While ^{14}C ages constrain the younger stratigraphy, older age assignments are primarily based on relating sedimentary cycles to the global Marine Isotope Stages (MIS) [34, 39, 40]. In addition to the age control, correlation with earlier investigated records allows us to expand the geographical coverage north- and eastwards. The resulting stratigraphic framework is used to discuss major sedimentation patterns along the transects and their implications for reconstructing Late Quaternary glacial/interglacial environments. More of the previously reported as well as unpublished Araon core data have been used for mapping sediment thickness (Supplementary Table 2).

Line-scan imaging

Line-scan images were acquired using a Jai CV L107 camera with RGB (red–green–blue) channels at 630, 535 and 450 nm, respectively, mounted to an AVAATECH core scanner. The camera contains three CCD sensors and a beam splitter to separate the RGB signal. Images were acquired with a down-core resolution of approx. 150 pixels per cm. The colour data have been calculated from a manually defined, undisturbed and representative image area as RGB and CIE $L^*a^*b^*$ values.

Physical properties

Physical properties provide initial core characterization with a very high vertical resolution. They are commonly measured on whole cores and can be used to define and interpret stratigraphical patterns, including a comparison with colour, lithology and other parameters such as data obtained from XRF scanning. Physical properties are also useful to link the cores to high-resolution sub-bottom acoustic profiles, thereby aiding the projection of core data from a single spot into larger spatial and temporal scales.

Onboard RV Polarstern and RV Araon data acquisition was carried out in 10 mm core intervals using a Multi Sensor Core Logger (MSCL, Geotek Ltd., UK). Details of data acquisition, calibration and corrections as well as equipment specifications are described in Jokat [41] and Kang et al. [42].

The wet-bulk density data presented here are based on gamma-ray attenuation. For calibration, a standard consisting of different proportions of aluminium and water as described in Best and Gunn [43] has been used. The general down-core gradient due to compaction is removed by curve-fit analyses using a second-order polynomial function and data are presented as WBD (g/ccm) residuals.

Magnetic susceptibility ($10e^{-5}$ SI) was measured using a Bartington MS-2C loop sensor (14 cm diameter), which was checked for possible drift above the top and below the bottom of the core by logging a 250-mm long water-filled liner as initial and final calibration piece, respectively. To calculate volume-specific magnetic susceptibility, data are corrected for loop sensor and core diameter. The down-core gradient has been removed (see above) and data are

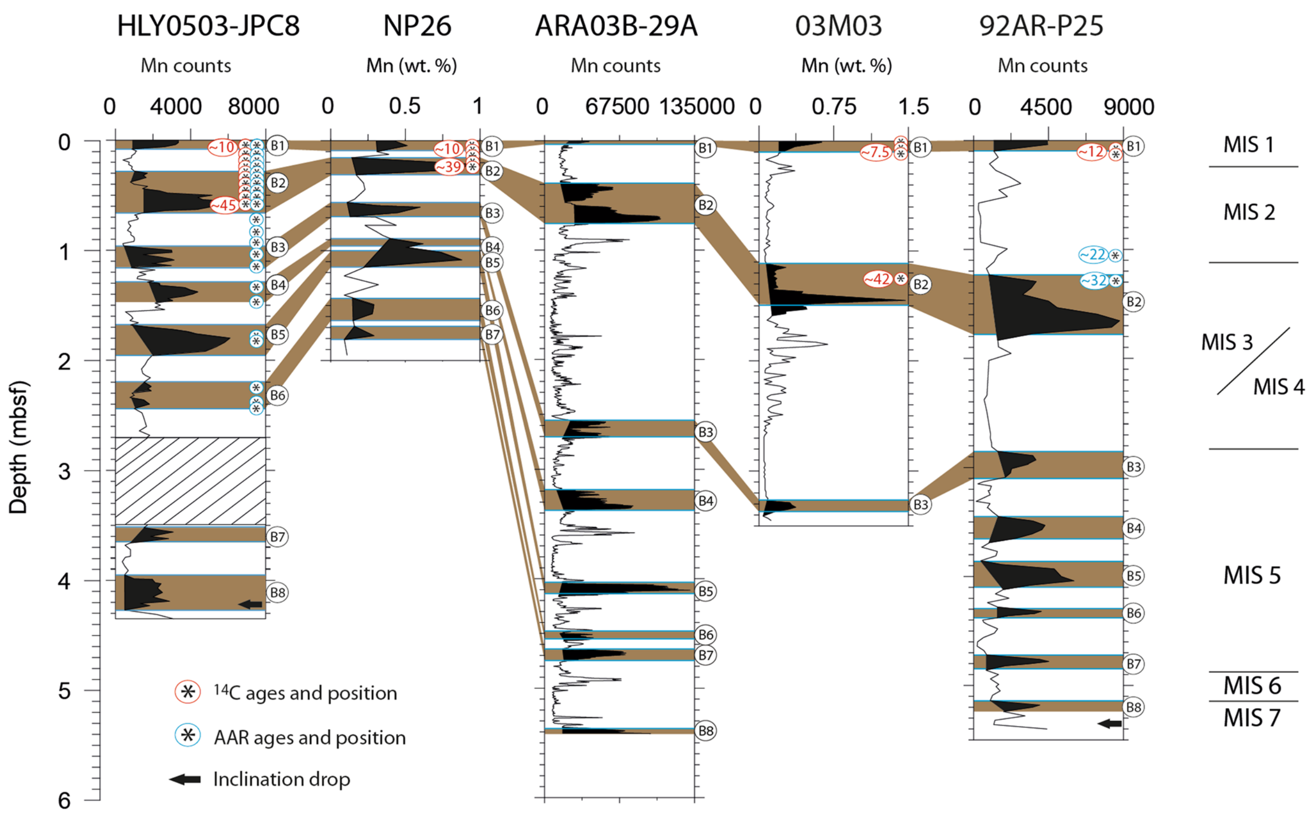

Fig. 2 Correlation of core ARA03B-29A (this study) to sediment records from or near the study area (Fig. 1) with developed age models including ^{14}C/AAR ages [12, 34, 39, 40]. Brown units are shaded and labelled B1–B8. Correlation is based on visual lithostratigraphy and Mn content reported in Mn counts (HLY503-JPC8, ARA03B-29A, 92AR-P25), and weight percentage (NP26, 03M03). Other stratigraphic data are not shown for presentation purposes. The hatched area marks the slump in core HLY0503-JPC8 [34]. Black arrow at the base of the HLY503-JPC8 and 92AR-P25 records indicate position of inclination drop as discussed in the text. Red and blue circles indicate position and ages of ^{14}C/AAR datings, respectively. Only selected ages representative for units B1 and B2 are presented; see source studies referred to above and Supplementary Table 1 for more detailed information

Table 1 Location and water depth of cores analysed in this study

Core name	Gear	Latitude	Longitude	Water depth (m)
PS72/340-5	KAL	77.60	– 170.51	2349
PS72/342-1	GC	77.60	– 176.65	820
PS72/343-2	GC	77.30	179.04	1225
PS72/344-3	KAL	77.61	174.54	1257
ARA03B-8	GC	76.60	– 160.78	2160
ARA03B-19	GC	77.96	173.03	1093
ARA03B-27	GC	75.51	178.69	677
ARA03B-28A	GC	76.21	– 179.16	1179
ARA03B-28B	GC	76.56	– 177.74	762
ARA03B-29A	GC	77.00	– 176.57	1430
ARA03B-30A	GC	77.14	– 171.76	1961
ARA06C-03	JPC	75.53	178.73	715

GC gravity core, *KAL* Kastenlot (box-shaped gravity core), *JPC* Jumbo Piston Corer

presented as volume-specific magnetic susceptibility ($10e^{-6}$ SI) residuals.

XRF analyses

High-resolution elemental analyses of RV Araon cores were performed on split cores by X-ray fluorescence (XRF) using an AVAATECH core scanner equipped with a rhodium (Rh) X-ray source and a Canberra X-PIPS Detector SXD15C-150-500 (resolution > 190 eV) at the Korea Institute for Geoscience and Mineral Resources (KIGAM). Each core section was scanned with three different instrumental settings (Table 2), and data were collected at down-core resolution of 5 mm. The cores recovered by RV Polarstern have been scanned at the Alfred Wegener Institute, Helmholtz Centre for Polar and Marine Research (AWI) using the same device but with down-core resolution of 10 mm. To avoid contamination of the detector and desiccation of the sediment, the split core surface has been covered with thin (4 µm) Ultralene® foil.

Table 2 Instrumental settings of the Avaatech XRF core scanner used in this study

Tube voltage (kV)	X-ray current (μA)	Resolution (cm)	Count time (s)	Filter
10	1200	0.5 (1)[a]	12	No
30	1500	0.5 (1)[a]	15	Pd-thick
50	1500	0.5 (1)[a]	20	Cu

[a]Number in brackets indicates the vertical resolution used for scanning RV Polarstern cores

To assure acquisition of highest quality XRF spectra, the sediment surface has been cleaned and smoothened, and wrinkles on and bubbles under the foil have been removed before the measurements. Four powdered standards were analysed prior to each core to monitor possible shifts in count intensities. Data were evaluated by analysis of X-ray spectra with the WinAxilBatch™ software (Canberra Eurisys Benelux) and are expressed semi-quantitatively as total counts, i.e. integrated peak areas. The total counts for each element have been normalized to Al, which presents a stable and abundant terrigenous element related to fine grained siliciclastic material. It is particularly useful in regions with high contributions of terrigenous detrital such as the Arctic Ocean and circumvents the effects of dilution [44]. However, we are aware of the selective intensity reduction of Al related to increased pore water contents, in particular in the upper part of the cores (see Ref. [45] for details), but assume a comparable influence on all analysed cores. Thus, results are presented as element count ratios.

Results

All studied cores are characterized by alternations of conspicuous dark brown intervals (indexed B1–B8) and brighter coloured, yellowish to greyish sediments (indexed G1–G7). The upper boundary of the dark brown units is usually distinct, while the lower boundary shows evidence for bioturbation (Fig. 3). We characterize the cores along the two transects using sediment colour, bulk density and magnetic susceptibility, along with stratigraphically distinct major elements (manganese and calcium) (Figs. 4, 5, 6, 7).

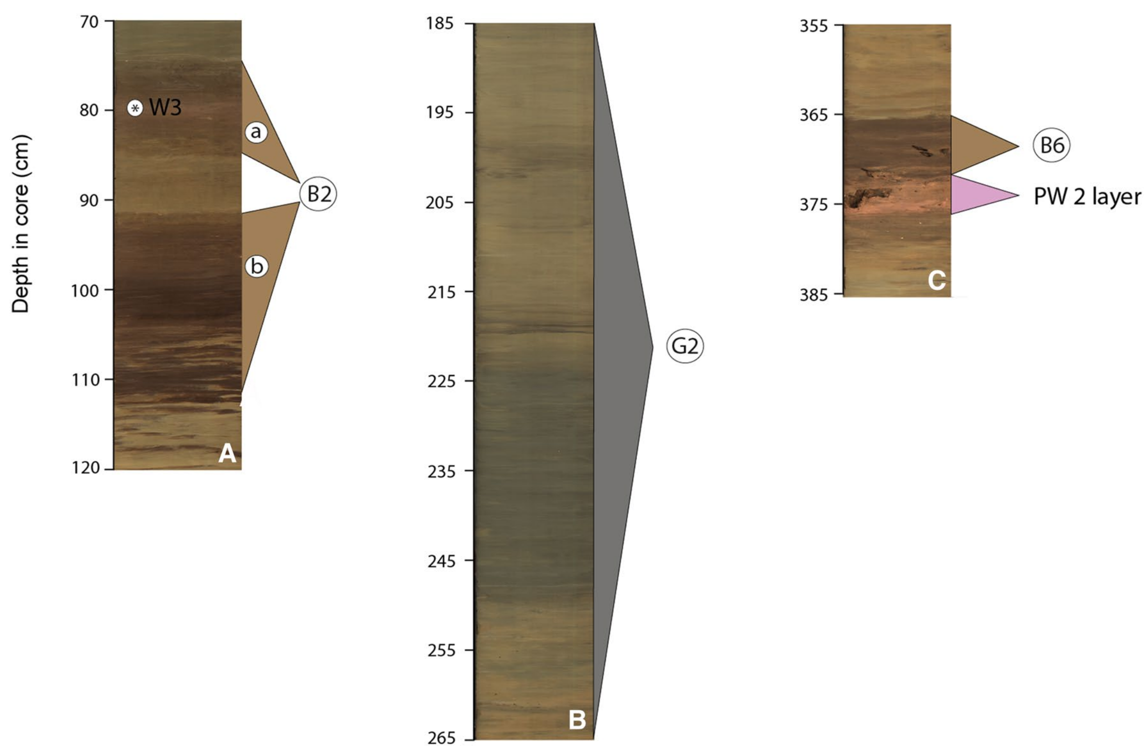

Fig. 3 High-resolution line-scan images from core ARA03B-30A showing representative examples for brown, yellowish-grey and pink–white units as discussed in the text. **a** Brown unit B2, showing the subdivision into B2a and B2b. Also note the distinct upper boundary of both subunits, while the lower boundary shows evidence of bioturbation. Pink–white layer W3 of Clark et al. [26] is visible within the upper part of B2 corresponding to B2a. **b** The yellowish-grey sediments deposited between the brown units. Shown here is unit G2, which is thickest grey unit observed in the study area. The dark grey colour in the middle part of the unit presents genuine glaciogenic sediment with more transitional yellowish-grey sediment above and below. **c** Pink–white layer PW2 of Clark et al. [26] located just below brown unit B6

Sediment colour

All analysed cores are characterized by cyclic down-core variations in sediment colour. In particular, the readily visible dark brown intervals are usually characterized by lightness value $L^* < 60$, and most exhibit distinct minima of ~ 55–50. The intercalated yellowish to greyish sediments are characterized by L^* commonly higher than 60 (Figs. 4, 6). In addition, the low L^* values within the brown intervals correspond to high a^* values (red–green colour space; not shown in Figs. 4, 6) allowing for unequivocal distinction of these intervals using sediment colour data.

Physical properties

A combination of wet-bulk density (WBD) and magnetic susceptibility (MS) records in all analysed cores displays stratigraphically consistent down-core variations. In general, the brown units are characterized by low WBD, which usually coincides with increased MS. However, this common pattern also includes intervals with strong negative correlations, as well as gradients in one parameter crossing positive or negative peaks in the other (Figs. 4, 6). These features can be traced across all analysed cores providing independent tie lines for stratigraphic correlation. In particular, brown unit B2 exhibits a very distinct minimum in WBD that correlates with a gradient in MS from higher to lower values. In contrast, brown units B3 and B5 show a clear anti-correlation between increased WBD and decreased MS. Brown unit B4 is characterized by a similar correlation, but the peak in MS seems to occur just prior to the minimum in WBD in most cores. Some other consistent features of the WBD and MS records provide additional correlation tie points. For example, WBD shows a distinct maximum associated with low MS values just below brown unit B2. A similarly increased WBD is observed above B3 and B4, along with increased MS identified in cores with sufficient resolution. Where sediment sections between the brown units are expanded, they are often characterized by minimal MS combined with a mostly constant WBD (dark grey shadings in Figs. 4, 6).

Distinct pink–white (PW) layers are usually characterized by a positive correlation of WBD and MS, often associated with distinct maxima in both parameters (Figs. 4, 6). A similar pattern is observed in intervals with elevated abundance of pinkish-white clasts or lenses (underdeveloped PW layers). This pattern is commonly observed in the vicinity of the brown units, typically occurring at their top or the base.

XRF Mn and Ca data

The Mn/Al ratio shows cyclic down-core variations with maximum values around 0.8–0.9 and typical background values < 0.5 in all analysed cores. All readily visible brown layers are characterized by increased Mn/Al ratios (Figs. 5, 7). Mn enrichment occasionally extends below their lower boundaries, often mottled as a result of bioturbation. Cores located closer to the East Siberian continental margin (e.g. PS72/343-2, PS72/344-3 and ARA03B-19; Fig. 1) also exhibit increased Mn/Al ratios in several intervals not confined to visible brown units.

Ca/Al ratios also display a distinct down-core pattern, where elevated values are generally related to or observed in the vicinity of the brown units across both transects (Figs. 5, 7). In addition, a clear increase in the magnitude of Ca/Al ratios (from 0.8 to 1) is observed from west to east in transect A and from south to north in transect B, respectively. Maximum values in the Ca/Al ratio, which may combine terrigenous (detrital) and biogenic Ca [31, 35], correspond to distinct PW layers or lenses/clasts. However, this relation is less obvious closer to the East Siberian continental margin due to a decreasing amount of readily visible PW layers/lenses. In general, Ca/Al peaks related to PW layers are also reflected by increased magnetic susceptibility (see above), which is consistent with observations from the Mendeleev and Alpha ridges [28].

Stratigraphic correlation

To overcome limitations of stratigraphic correlations based on just one type of proxies, we utilize a combination of multiple parameters (L^*, WBD, MS, Mn/Al, Ca/Al) for a stratigraphic alignment of cores under study across the western Arctic Ocean off the East Siberian to Chukchi margins. The primary tie lines for the correlation are the brown units and the pink–white layers, expressed in multiple parameters (Figs. 4, 5, 6, 7).

Transect A: East Siberian margin towards the Northwind Ridge

The uppermost few centimetres are usually characterized by a dark brown colour, low L^* values and increased Mn/Al ratios. Unfortunately, the WBD and MS signal are somewhat obscure due to effects of liner caps at the section ends when logging whole cores. This surficial brown unit B1 is recognized in most cores, but is generally compressed, possibly due to effects of gravity coring. Unit B1 is not recovered in the Kastenlot cores PS72/344-3 and PS72/340-5, but is well preserved in corresponding box cores (see Ref. [13]).

The subsequent brown unit B2 is characterized by a distinct minimum in WBD that corresponds to a gradient in MS accompanied by minimum L^* values and a maximum in Mn/Al ratio (Figs. 4, 5). A combination of these features allows for an unambiguous correlation, further supported by a distinct double peak in Ca/Al ratio within B2. In cores located on the eastern (Laurentide) side of transect

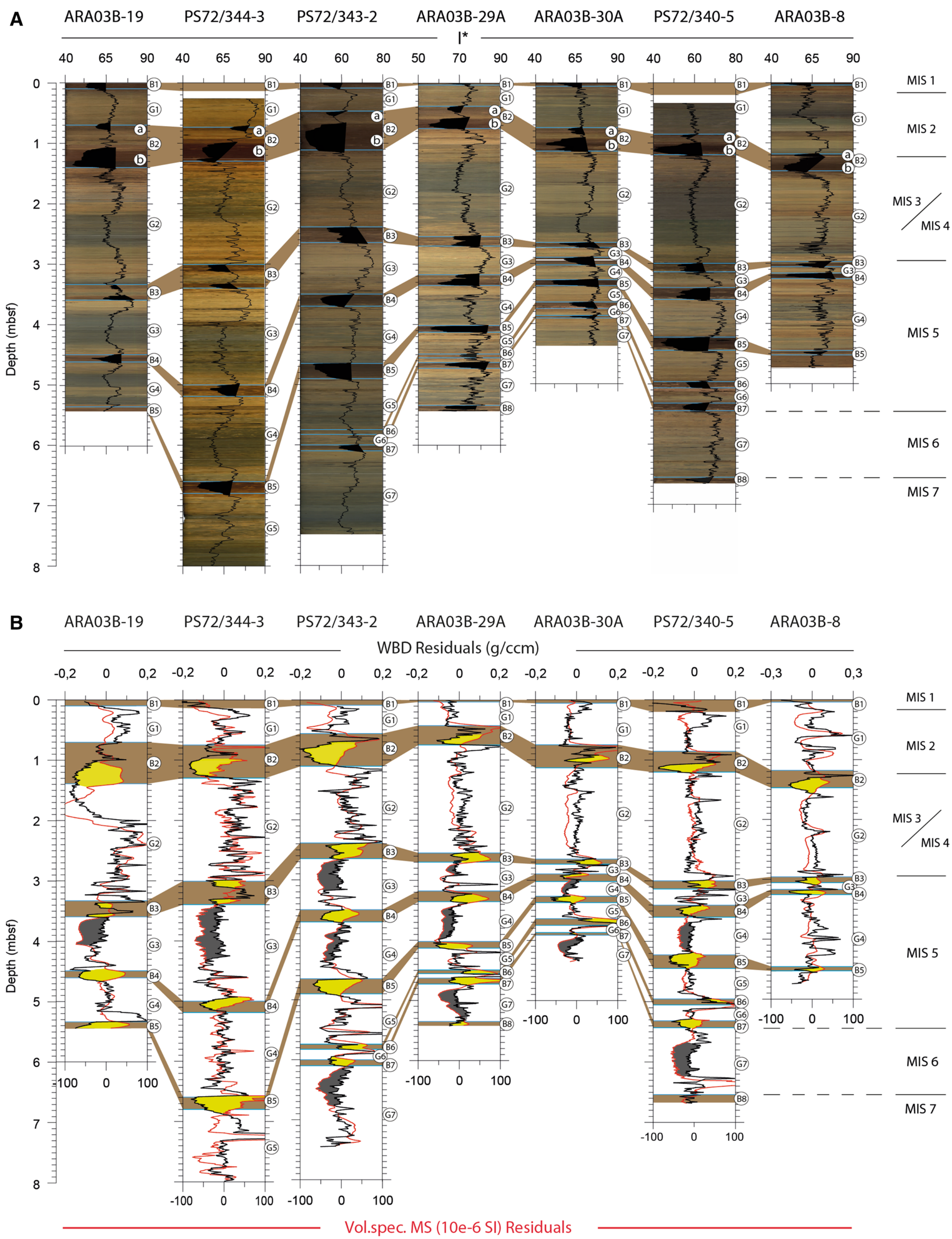
A
ARA03B-19
PS72/344-3
PS72/343-2
ARA03B-29A
ARA03B-30A
PS72/340-5
ARA03B-8
I*
Depth (mbsf)
MIS 1
MIS 2
MIS 3
MIS 4
MIS 5
MIS 6
MIS 7
B
WBD Residuals (g/ccm)
Vol.spec. MS (10e-6 SI) Residuals

◂**Fig. 4** Stratigraphic core correlation across transect A from the Kucherov Terrace to Northwind Basin. Brown units are shaded and labelled B1–B8. Yellowish-grey units are labelled G1–G7. **a** Correlation based on sediment lightness (*L**); also shown are high-resolution line-scan core images. Subdivision of B2 in B2a and B2b [according to ref. 13] is exemplified. **b** Correlation based on wet-bulk density (g/ccm) and volume-specific magnetic susceptibility (SI units)

A (ARA03B-30A, ARA03B-8, PS72/340-5; Fig. 1), the increased Ca/Al ratio is expressed by a clearly visible PW layer (or lenses); a consistent feature in many cores from the western Arctic (layer W3 in the lithostratigraphy of Ref. [26]). A correlative PW layer has not been visibly encountered in cores west of the Mendeleev Ridge, but is clearly expressed in Ca/Al ratios associated with the occurrence of PW lenses/clasts (Fig. 5). In addition, PW layer W3 is characterized by significantly increased MS values.

In most cores, unit B2 can be subdivided into two subunits (B2a and B2b according to Ref. [13], and exemplarily shown in Figs. 3, 4a, 5a) based on the *L** value, and Mn/Al. In addition, subunit B2a exhibits elevated WBD, often associated with increased MS, in most cores. The subdivision of brown unit B2, however, is more obscure in cores with lower sedimentation rates, likely due to bioturbation mixing.

The correlation of brown unit B3 is straightforward from the Mendeleev Ridge to the Chukchi Borderland (Figs. 4, 5). Just below B3, cores west of the Mendeleev Ridge (ARA03B-19, PS72/344-3, PS72/343-2, ARA03B-29A) are characterized by an interval of generally uniform MS and WBD, with the latter being constantly higher than MS (dark grey-shaded area in Fig. 4b). This interval terminates with a peak in WBD just above brown layer B4 that can be traced across all cores, including those located east of the Mendeleev Ridge, and therefore, provides an additional correlation feature. Further support for a reliable correlation is provided by a Ca/Al peak associated with B3 in all cores (Fig. 5). This peak is visually well-expressed as a PW layer in the eastern part of the transect and is associated with a more sporadic occurrence of individual clasts towards the East Siberian margin. Cores from the Kucherov Terrace (ARA03B-19, PS72/344-3) show a subdivision of B3 similar to that observed in B2, which is likely an effect of higher sedimentation rates towards the East Siberian margin. These cores also exhibit two clearly distinguishable Ca/Al peaks.

Brown unit B4 is clearly recognizable by a distinct anti-correlation of WBD and MS and the observed behaviour of *L** (minimum) and Mn/Al ratio (maximum), which allows a reliable correlation from west to east (Figs. 4, 5). In addition, B4 exhibits increased Ca/Al ratios, but of a smaller magnitude than within units B2 and B3. In cores east of the Mendeleev Ridge, the Ca/Al peak in unit B4 is only displayed by scattered clasts and has no visible representation in cores closer to the East Siberian margin. Similar to sediment underlying unit B3, the grey unit below B4 is characterized by a minimum of MS superimposed on generally constant WBD in some of the cores (grey shading in Fig. 4b).

Similar to unit B4, brown unit B5 is characterized by a clear anti-correlation of WBD and MS and easily recognizable in the *L** and Mn/Al records in all cores, thus allowing a straightforward correlation from the Northwind Ridge to the Kucherov Terrace (Figs. 4, 5).

While all cores of transect A recovered sediments down to at least unit B5, four of the cores penetrated older brown units B6 and B7 (Figs. 4, 5). In contrast to unit B7, which can be distinctly correlated across transect A, the identification of B6 is somewhat more ambiguous. In particular, in cores ARA03B-29A and PS72/343-2 correlation based on *L** and Mn/Al is not obvious, but a PW layer at the base of B6 is clearly visible in all cores. It is expressed in a maximum in the Ca/Al ratio and a combination of high WBD and MS values, thus supporting correlation of cores ARA03B-29A and PS72/343-2. This PW layer corresponds to the PW2 layer in the lithostratigraphy of Clark et al. [26] that has also been described in multiple cores from both Mendeleev and Northwind Ridges in previous studies [12, 13, 34]. The sediment below unit B7 is, similar to sediment underlying units B3 and B4, characterized by a minimum of MS superimposed on generally constant WBD (grey shading in Fig. 4b) providing additional constraints on core correlation. Brown unit 8 has only been recovered in cores ARA03B-29A and PS72/340-5 (Figs. 4, 5).

Transect B: north from the East Siberian margin along the Mendeleev Ridge

Similar to transect A, the uppermost few cm (unit B1) are characterized by a dark brown colour, low *L** values and increased Mn/Al ratios in all cores, but are somewhat compressed due to gravity coring effects (Figs. 6, 7). The subsequent interval corresponding to unit B2 is easily identifiable in the *L** (minimum) and Mn/Al (maximum) record. It is characterized by a distinct WBD vs. MS pattern with a MS gradient from higher to lower values running through a minimum in WBD, as well as distinct subdivision into subunits B2a and B2b (exemplarily shown in Figs. 3, 6a, 7a) and a conspicuous double peak in the Ca/Al ratio, as described for transect A.

Only cores ARA03B-29A and PS72/342-1 recovered brown units B3 and B4 (Figs. 6, 7), which can be correlated straightforwardly as in transect A. The ~ 1-m-long bottom part of PS72/342-1 is composed of stiff, over-consolidated sediment interpreted as a diamicton [13]. Stein et al. [13] tentatively identified brown units B5 and B6 in this part of the core based on lithostratigraphic description. Our new data clearly show that there are no indications for ‘real’ brown units below brown unit B4 in core

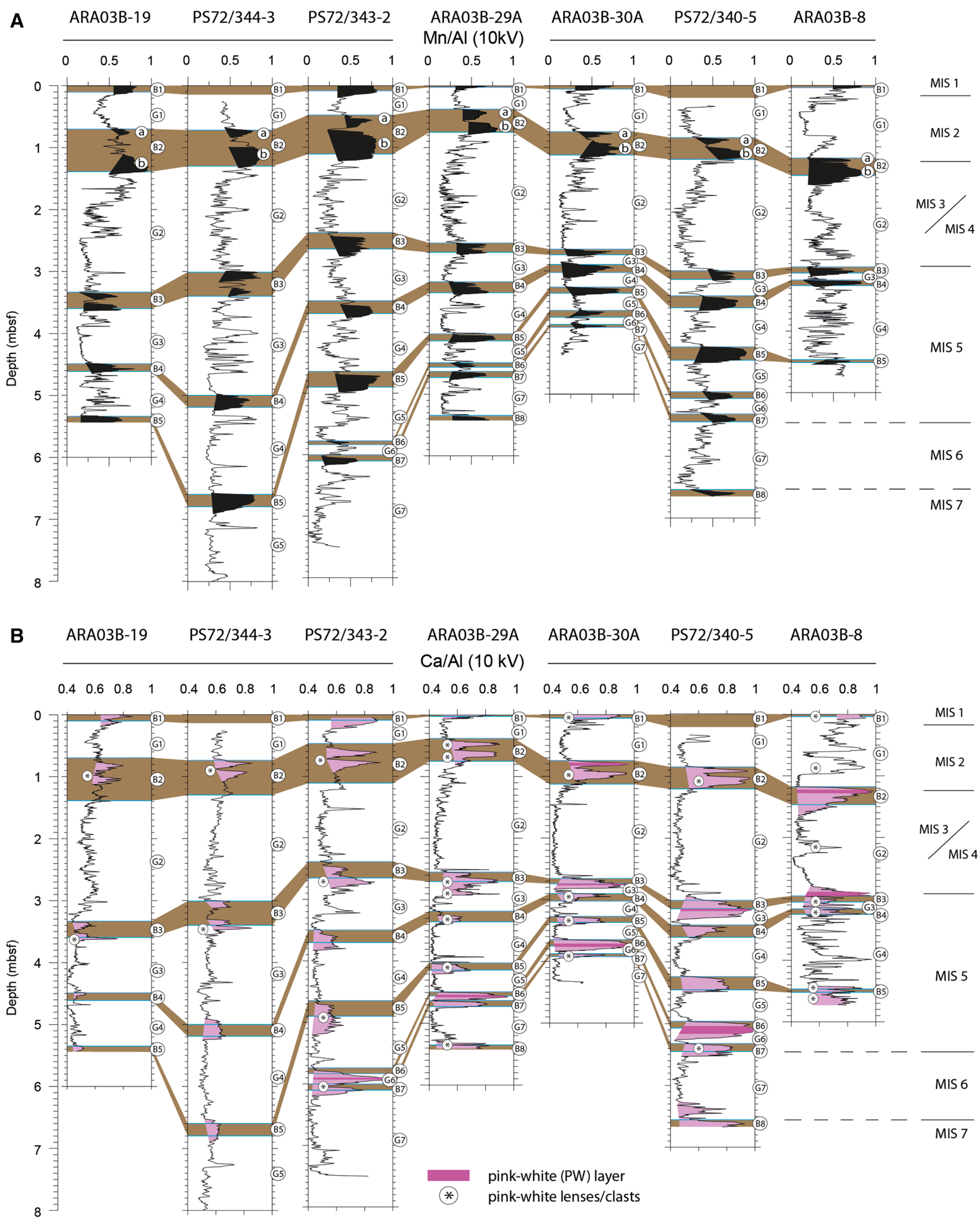

Fig. 5 Stratigraphic core correlation across transect A from the Kucherov Terrace (West) to Northwind Basin (East). Brown units are shaded and labelled B1–B8. Yellowish-grey units are labelled G1–G7. **a** Correlation based on Mn/Al ratio. Subdivision of B2 in B2a and B2b (according to Ref. [13] is exemplified. **b** Correlation based on Ca/Al ratio. Visible pink–white are indicated by dark pink shading, pink–white clasts and lenses are indicated by asterisks

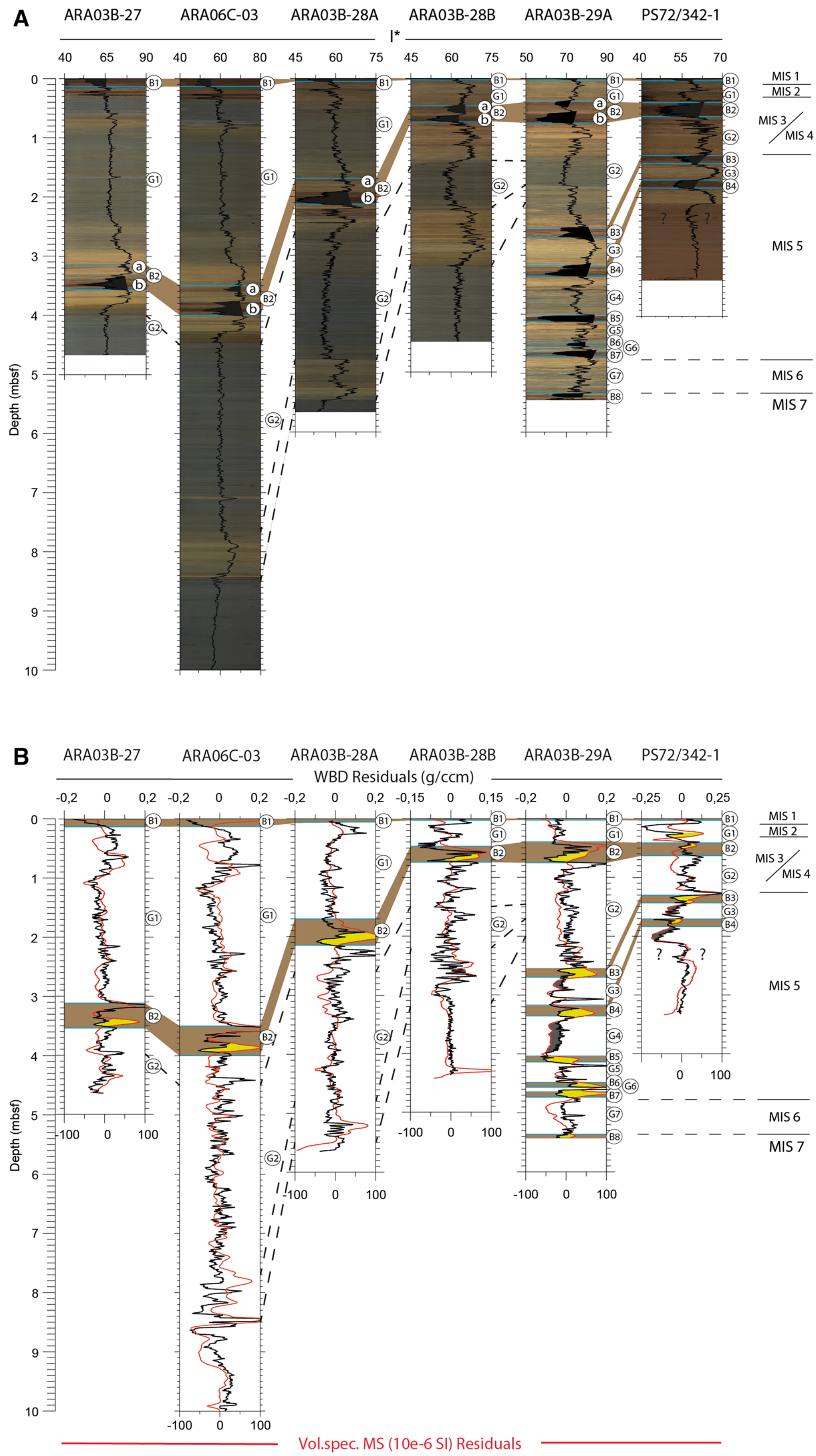

Fig. 6 Stratigraphic core correlation across transect B from the East Siberian continental margin northwards along the Mendeleev Ridge. Brown units are shaded and labelled B1–B8. Yellowish-grey units are labelled G1–G7. **a** Correlation based on sediment lightness (*L**). Also shown are the high-resolution line-scan core images. Subdivision of B2 in B2a and B2b (according to Ref. [13]) is exemplified. **b** Correlation based on wet-bulk density (g/ccm) and volume-specific magnetic susceptibility (SI units). Dashed lines show additional correlation ties within expanded grey unit 2

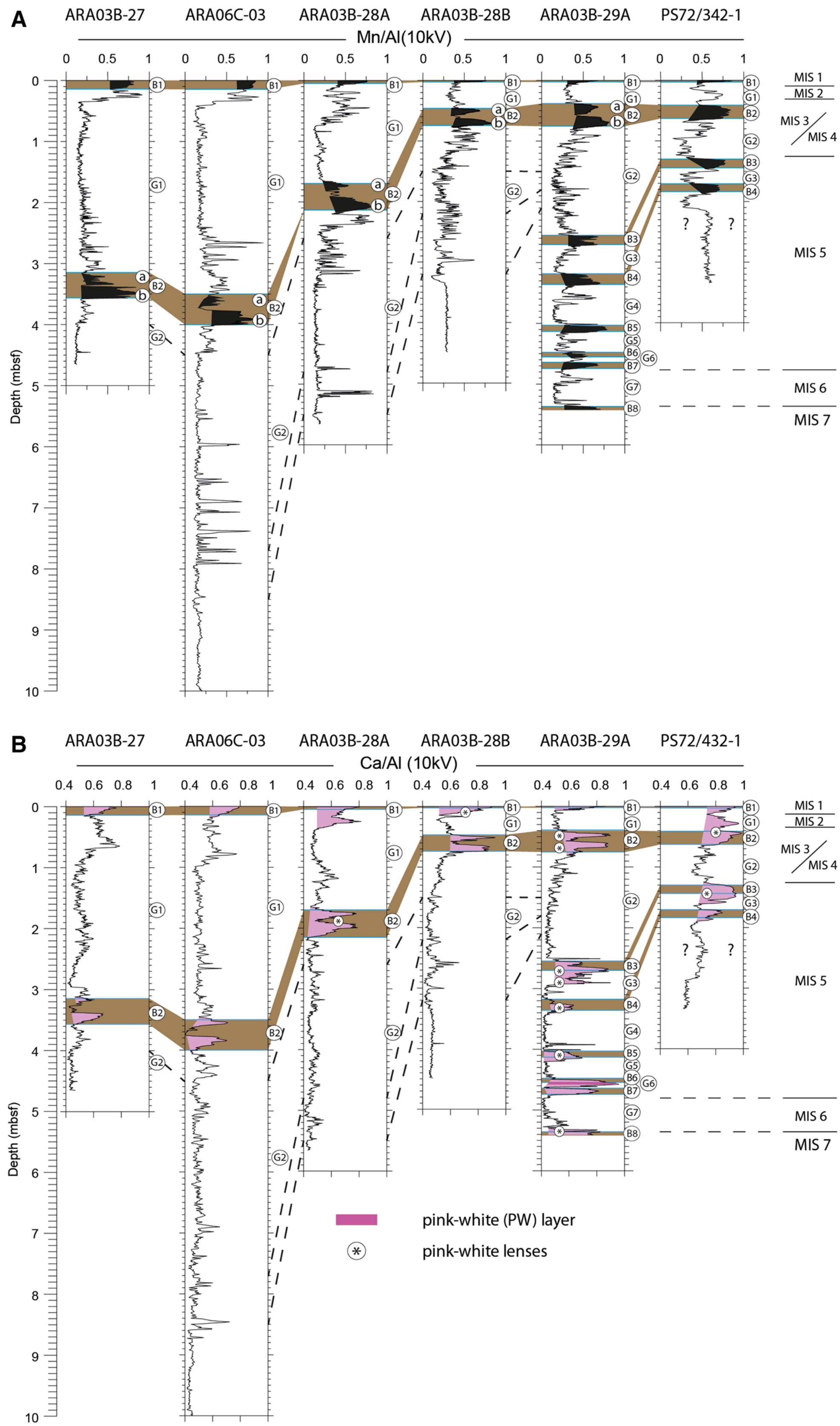
A
ARA03B-27
ARA06C-03
ARA03B-28A
ARA03B-28B
ARA03B-29A
PS72/342-1
Mn/Al(10kV)
Depth (mbsf)
MIS 1
MIS 2
MIS 3
MIS 4
MIS 5
MIS 6
MIS 7
B
ARA03B-27
ARA06C-03
ARA03B-28A
ARA03B-28B
ARA03B-29A
PS72/432-1
Ca/Al (10kV)
Depth (mbsf)
pink-white (PW) layer
pink-white lenses

◀**Fig. 7** Stratigraphic core correlation across transect B from the East Siberian margin northwards along the Mendeleev Ridge. Brown units are shaded and labelled B1–B8. Yellowish-grey units are labelled G1–G7. **a** Correlation based on Mn/Al ratio. Subdivision of B2 in B2a and B2b (according to Ref. [13]) is exemplified. **b** Correlation based on Ca/Al ratio. Dashed lines show additional correlation ties within expanded grey unit 2. Visible pink–white are indicated by dark pink shading, pink–white clasts and lenses are indicated by asterisks

PS72/342-1 (Figs. 6, 7), highlighting the value of a multi-parameter correlation approach. The dark brown colour of the basal deposit in PS72/342-1 is likely attributable to glacial reworking of pre-glacial marine strata of brown colour as described for this location in Stein et al. [13]. This also explains the elevated Mn/Al ratio in this part of the core. None of the cores retrieved closer to the Siberian shelf penetrate down to the stratigraphic level of unit B3 due to higher sedimentation rates.

In summary, core correlation is straightforward from the East Siberian margin towards the Northwind Ridge, showing that all cores along this W–E transect A penetrated to at least unit B5 (Figs. 4, 5). This lithostratigraphy highlights the value of combining multiple parameters (L^*, WBD, MS, and Mn and Ca contents) for core-to-core correlations, which is especially effective in an area with a generally consistent depositional history. Cores recovered from transect B stretching from south to north along the Mendeleev Ridge demonstrate a convincing correlation to unit B2. Most cores near the East Siberian margin; however, do not reach the subsequent brown unit B3 (Figs. 6, 7).

Discussion

Age assignment

Due to their vigorously bioturbated nature and elevated content of micro- and nannofossils, dark brown units in Quaternary Arctic Ocean sediments are commonly interpreted as interglacial or major interstadial deposits (e.g. [22, 36, 46, 67 and references therein). In this approach, the surficial brown unit B1 represents the Holocene, which is corroborated by numerous AMS ^{14}C dates typically showing the age of 10–12 ka at its base in sediment cores from various regions of the Arctic Ocean (Fig. 2; 12, 34, 39–40, 47, see also compilation of ^{14}C ages in Refs. [46, 67]). Similarly, the subsequent brown unit B2 (in some cases identified as two subunits, B2a and B2b) is AMS ^{14}C/AAR dated in multiple cores from the major ridges and basins with a consistent pattern of ages around 40–45 ka for its base (e.g. [11, 12, 34, 39, 40, 46, 47]). The stratigraphically important pink–white layer (W3) in the upper part of B2 (often between B2a and B2b; Fig. 3) has an age of around 40 ka [34]. These ages indicate that this conspicuous brown unit represents a prominent interstadial within MIS 3, rather than MIS 5 as believed in earlier stratigraphic studies (e.g. [26, 30]).

Beyond the range of ^{14}C dating, age control for Pleistocene Arctic Ocean sediments remains challenging [9, 13]. Age models in most recent studies mainly rely on cyclostratigraphy [35, 48], reinforced by paleomagnetic correlations and a few biostratigraphic datums, which mostly have only intra-Arctic significance [22]. An initial optical stimulated luminescence (OSL) study further corroborates the age model for upper Pleistocene sediments from Lomonosov Ridge [18], while no absolute age data other than ^{14}C are available in the western Arctic Ocean. Some constraints on a longer upper Pleistocene stratigraphy are provided by AAR data [34, 49], but these ages rely on the ^{14}C-based calibration and require an independent age control in older sediments. These limited chronostratigraphic constraints result in different age estimates for some of the stratigraphic horizons. In particular, varying ages have been proposed for units B3–B5 in the study area. Based on correlations with records from the Lomonosov Ridge (see Refs. [34, 49] for details), along with abundance maxima of some benthic (e.g. *Bulimina aculeata*) and planktonic foraminifers (peaks of subpolar species) in the Mendeleev Ridge core HLY0503-08JPC (Fig. 1) brown units B3 and B4 have been proposed to have a MIS 5a age [9, 34]. Conversely, Backman et al. [50] assigned this age to unit B5 (including the same core) based on the interpreted distribution of calcareous nannofossils with Atlantic affinity such as *Emiliania huxleyi* and *Gephyrocapsa* spp. Accordingly, the conspicuous horizon with PW layer/lenses near the bottom of B3 (or just below it), was estimated to be close either to the MIS 5/4 boundary (~70 ka; Refs. [9, 34]) or the MIS 4/3 boundary (~55 ka; Ref. [50]). We note that unlike abundant foraminifers in brown units of the upper Quaternary, calcareous nannofossil numbers in the western Arctic Ocean sediments are overall very low and strongly depend on preservation conditions, so that their down-core variation should be treated with caution. In particular, the occurrence of species, which may have an Atlantic affinity, but are not unique for one specific time interval (other than the *E. huxleyi* zone covering MIS 1–7), can be hardly used for discriminating between interglacials or major interstadials, such as MIS 3, 5a, and 5c. Regardless of the exact ages of these biostratigraphic constraints, which might be controlled by intra-Arctic rather than global factors, the integrated stratigraphy presented here demonstrates a consistent, thick, yellowish-grey unit between brown units B2 and B3 (Figs. 3, 4a, 6a). These yellowish to grey sediments are commonly attributed to glaciogenic environments [9, 12, 13, 34–36], which justifies their assignment to MIS 4/3, deposited just beyond the reach of ^{14}C dating. This stratigraphy further suggests that yellowish-grey units occurring in these cores at lower intervals represent older glacial events such as intra-MIS 5 and MIS 6.

There seems to be a consensus on the correlation of unit B7 with MIS 5e in the Mendeleev Ridge area based on foraminifera [9, 12, 34] or nannofossils [50]. This inference is consistent with the abundance of subpolar planktonic foraminifers and the occurrence of coccolithophores in this unit in core PS72/340-5 from the Chukchi Basin [13]. We note, however, the need for an independent age control for this paleoclimatically critical interval (last interglacial).

A major detrital carbonate layer, clearly visible between B6 and B7, corresponds to the PW2 layer in the lithostratigraphy of Clark et al. [26] and is related to increased detrital carbonaceous IRD supply caused by disintegration of the extended Laurentide Ice Sheet (e.g. [32] and references therein). The PW2 layer is a ubiquitous feature in sediment cores from the western Arctic Ocean, especially closer to the Laurentide margin, but becomes less obvious towards the East Siberian margin (e.g. [9, 12, 13, 26, 27, 31–36]). While a decrease in detrital carbonates in cores distal to the Laurentide source relates to background sedimentation and iceberg drift pathways (see below), this interval is still easily identifiable by its Ca content in distal cores from the East Siberian margin (this study; [9]). Stein et al. [13] assigned the PW2 layer age to MIS 5d (105–115 ka). However, this age assignment is arbitrary, not supported by any additional chronostratigraphic constraints. Similarly, the ages of the overlying brown units B5 and B6 cannot be confidently assigned to a particular interstadial within MIS 5.

Unit B8 recovered in cores ARA03B-29A and PS72/340-5 has been assigned in earlier studies to the upper part of MIS 7 [13, 34, 40]. A prominent drop in paleomagnetic inclination has consistently been observed just below B8 in multiple Arctic Ocean cores including HLY0503-08JPC and 92AR-P25 [9, 34, 40]. This feature, originally regarded as a polarity inversion [26], has been later reinterpreted as an excursion within MIS 7 [13, 16, 19], although a diagenetic nature of this change has also been suggested [20]. We note that the stratigraphic interpretation of the lower part of MIS 5 in HLY0503-08JPC is complicated by a slump between brown units that could be attributed to B7 and B8 (Fig. 2), which places the latter within MIS 6 [34]. However, a careful comparison with nearby records indicates that this unit belongs to B7, likely separated from its top part by the slump (Polyak, unpubl.), which places the actual B8 into MIS 7.

Depositional environments and sedimentation rates

The main lithological units distinguished in all cores (Fig. 3) are the brown units (B1–B8), intercalated yellowish-grey sediments (G1–G7) and the detrital carbonate-rich white and pink–white layers (PW and W layers), which characterize generic variety of depositional environments in the study area. In addition to low L^* and WBD, increased Mn contents, and distinct upper and bioturbated lower boundary, brown units across the western Arctic Ocean have characteristically high numbers of foraminifers, at least in the upper Quaternary, and low to moderate amount of ice-rafted debris (IRD) [9, 12, 13, 26, 27, 31, 33, 34, 37]. Therefore, these ubiquitous layers have been generally associated with interglacial and/or major interstadial conditions. The intercalated yellowish-grey units, characterized in the present data set notably by lower Mn/Al ratios, are inferred to represent glacially related environments [9, 12, 13, 27, 33–37]. The distinct pink–white layers (PW) or lenses are characterized by peaks in Ca contents and a positive correlation of WBD and MS, often with maxima in the latter, and maximum values in the Ca/Al ratio. These marker horizons have been shown to be largely composed of Palaeozoic dolomites originating from the Canadian Arctic Archipelago [29, 32] and interpreted pulses of iceberg discharge from the Laurentide Ice Sheet during disintegration events [9, 12, 13, 27, 31–33, 37].

To illustrate the general trends in spatiotemporal distribution of the major depositional environments, sediment thickness has been mapped across the study area for readily identified lithostratigraphic intervals roughly corresponding to MIS 1 to late MIS 3, MIS 3/4, and MIS 5 (Fig. 8a–c). This mapping allows us to evaluate sedimentation rates, depositional pathways, and principal provenance centres.

Differences in depositional patterns and sedimentation rates in the western Arctic Ocean are usually attributed to a combination of transportation distance from sediment sources at the continental margins and sea-ice concentrations along with associated melt-out rates [9, 13]. Thus, higher deposition revealed in cores from the southern part of the study area is consistent with more material from the continental shelves reaching these sites than the cores further north, which is especially pronounced in the glacial, grey-coloured units (Figs. 4, 5, 6, 7). Increased proximity may be related to shorter distance to paleo-shorelines at lower sea levels and/or grounding lines of the East Siberian ice sheets [6, 7]. In addition, sea-ice concentrations are highest towards the central parts of the basin while melting of sea ice is more pronounced closer to the ice margin [51], resulting in higher sedimentation rates towards the continental shelves. This pattern is likely strengthened by a longer residence time in the Beaufort Gyre circulation [51]. A generally restricted deposition at the submarine ridges is not only related to source proximity and thick sea-ice cover in the interior of the Arctic Ocean but, may also be enhanced by subsurface/bottom currents, which cause winnowing or by-passing of fine sediments and their deposition in the deeper basins [28, 34].

The prevailing long-term sedimentation pattern in the study area is characterized by an overall increase in sedimentation rates with increasing proximity to the continental margins, thus from east to west and from north to south (Figs. 4, 5, 6, 7, 8). While the thickness variation of overall

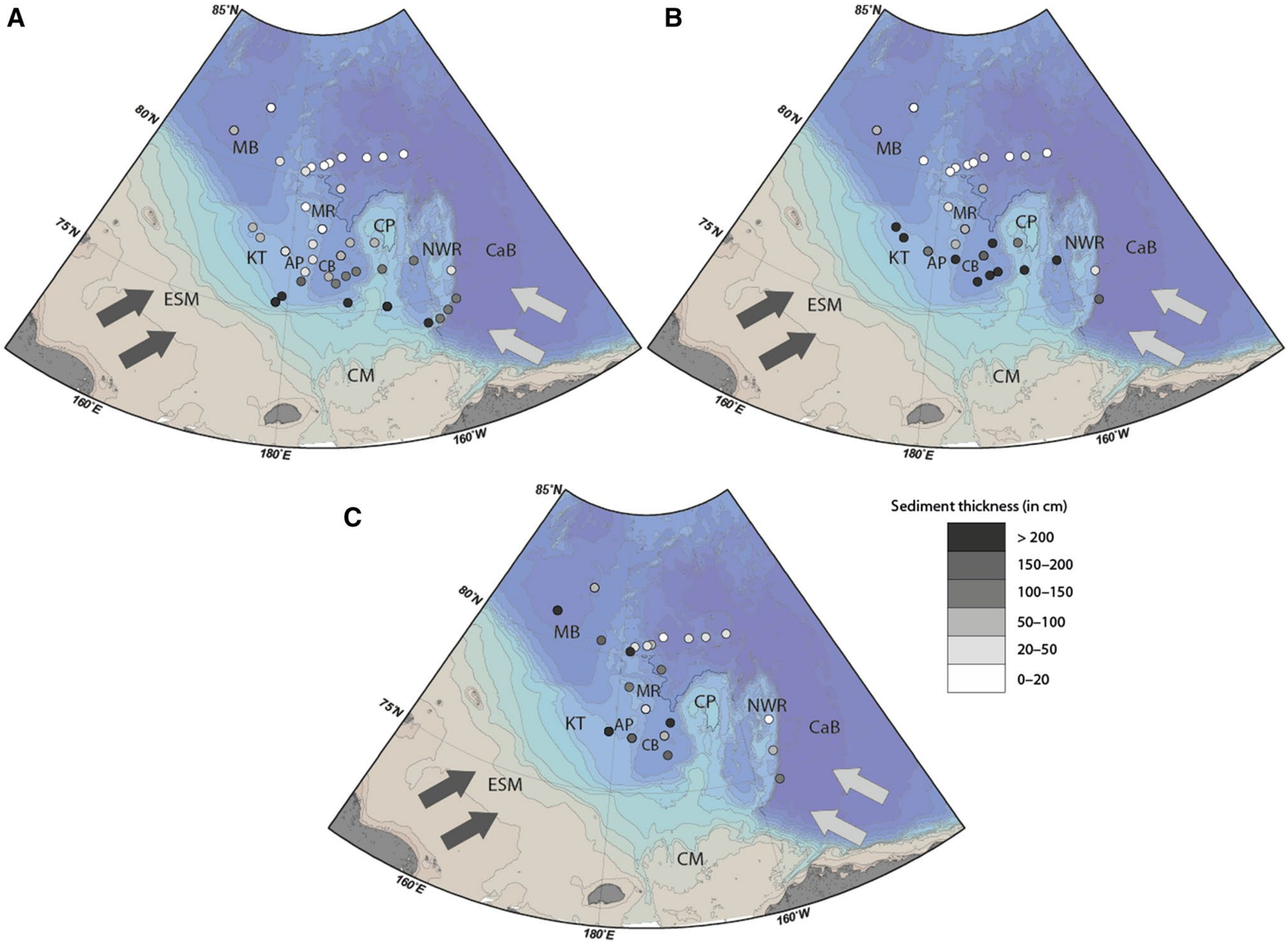

Fig. 8 Sediment thickness distribution for selected time intervals (see also Figs. 3, 4, 5, 6): from core top to unit B2 top (**a**) B2 to unit B3 top (**b**) and from B3 to PW 2 layer (**c**), roughly corresponding to MIS 1 to late MIS 3, MIS 3/4, and MIS 5, respectively. See text for more details on age control and Supplementary Table 2 for source data. Inferred sediment inputs from North America and Siberia are indicated by dark and light grey arrows, respectively. *AP* Arliss Plateau, *CaB* Canada Basin, *CB* Chukchi Basin, *CM* Chukchi margin, *CP* Chukchi Plateau, *ESM* East Siberian margin, *KT* Kucherov Terrace, *MB* Makarov Basin, *MR* Mendeleev Ridge, *NWR* Northwind Ridge

comparatively thin brown units is relatively small spatially, intercalating yellowish-grey units, largely related to glacial environments, show much more variable distribution. Their sedimentation rates are typically highest near the East Siberian margin, progressively decreasing northwards along the Mendeleev Ridge, and towards the Canada Basin. The lowest sedimentation rates are recorded in cores from the northern and eastern parts of the Mendeleev Ridge and Canada Basin further east (Fig. 8). A similar south–north and west–east decrease in sedimentation rates occurs in cores from the Northwind Ridge and the adjacent Alaska margin [9, 31], and a transect from the Makarov to Canada Basin across the Mendeleev Ridge [13].

While grey units between B1/B2 and B2/B3 (G1 and G2) are generally uniform in thickness on the latitudinal transect A, with unit G2 having a larger thickness of up to 2 m, unit G3 (between B3 and B4) is clearly thickening towards the East Siberian margin (Figs. 4, 5). This unit was deposited during either glacial MIS 4 or interstadial MIS 5a, according to the age models of Backman et al. [50] or Adler et al. [34] and Polyak et al. [9], respectively. The latter interpretation is consistent with an outburst of an ice-dammed lake in northern Siberia around ~ 77 ka inferred from a well-resolved sedimentary record from the Barents Sea slope in the eastern Arctic Ocean [53]. A noticeable decrease in the thickness of this unit eastwards possibly suggests relatively low sediment inputs from the Laurentide Ice Sheet by way of the Beaufort Gyre. Peaks in Ca/Al ratio related to abundance of detrital carbonates at the bottom and top of this unit in more eastern cores evince episodes of increased Laurentide IRD delivery (Fig. 4), while the condensed section inbetween indicates strongly reduced sediment inputs. An increase in sedimentation rates towards the East Siberian margin in cores west of the Mendeleev Ridge clearly indicates a proximity to the major sediment source.

In contrast to a relatively uniform thickness of units G1 and G2 across transect A, both units decrease significantly across transect B from south to north (Figs. 6, 7, 8). This pattern may indicate a closer proximity of cores from the southern part of the Mendeleev Ridge (Arliss Plateau) to the ice-sheet margin in comparison with cores located further northwest (Kucherov Terrace) during MIS 2 and 3.

Brown units may also display some degree of thickness variability, although not as large as glacial-related units. In particular, unit B2 thickens west and southwards in both transects, suggesting higher sedimentation rates near the East Siberian margin at interstadial environments within MIS 3. This pattern can be related to higher inputs from the margin and/or reduced sea-ice cover, as compared to the cores east of the Mendeleev Ridge, where sedimentation is controlled by thicker sea ice within the Beaufort Gyre circulation.

The importance of the main surface circulation systems (Beaufort Gyre and Transpolar Drift, Fig. 1) for sea ice and iceberg drift trajectories, and thus sedimentation patterns, is also corroborated by the spatial distribution of readily visible detrital carbonates (PW layers) across the western Arctic (Figs. 5, 7). Icebergs and meltwater pulses from collapse events of the NW sector of the Laurentide Ice Sheet were transported by the Beaufort Gyre towards the Chukchi Borderland and Mendeleev Ridge, then further north towards the Alpha Ridge [9, 29, 31, 54]. The occurrence of dolomite clasts/lenses, in particular PW2 and W3, as far west as the Kucherov Terrace near the East Siberian margin may suggest an expanded Beaufort Gyre during these events in comparison to the present day circulation (e.g. [55]).

Interestingly, cores from the East Siberian margin (PS72/343-2, PS72/344-3 and ARA03B-19) exhibit intervals with increased Mn/Al ratios that are not reflected in low L^* values, and thus not confined to brown units (Figs. 4, 5). In particular, some intervals within grey sedimentary units G2 and G3 show Mn enrichment beyond background values. This pattern in the upper part of unit G2 in core 03M03 from the Chukchi Basin (Fig. 2) was shown to be related to the presence of Fe–Mn micronodules [39]. A similar Fe–Mn micronodule enrichment was also found in correlative sediments in the Northwind Basin (T. Zhang, pers. comm., 2017), indicating that their formation may be characteristic for a specific deglacial environment.

Implications for timing and extent of ice advances at the East Siberian margin

Niessen et al. [5] and Jakobsson et al. [7] presented evidence for recurrent ice grounding on the East Siberian margin and adjacent Arliss Plateau based on swath bathymetry and sub-bottom profiles (Fig. 1). Four sets of Mega Scale Glacial Lineations (MSGL), presumably formed by the movement of grounded ice-sheets/-shelves, have been distinguished at the Arliss Plateau [5]. The youngest and oldest sets extend to ~ 950 and ~ 1200 m below present sea level (mbpsl), respectively. The grounding line corresponding to the youngest event, identified at the northern tip of the plateau, was interpreted as the most recent grounding extent of an ice-sheet/ice-shelf advance from the East Siberian margin [5].

To constrain the timing of these grounding events, sediment cores ARA03B-28A (1179 mbpsl) and ARA03B-28B (762 mbpsl) have been collected on the Arliss Plateau within the oldest and youngest MSGL sets, respectively (Fig. 1). Both cores can be unambiguously correlated to each other and to core ARA03B-29A based on visual lithostratigraphy, physical properties, and XRF data presented above (Figs. 6, 7), and thus to age-constrained cores from prior studies (Fig. 2). Neither core ARA03B-28A nor −28B reach brown unit B3, but end in an extended grey unit G2 (Fig. 6a), probably deposited during or just after the last glacial grounding event. As discussed above, while the exact age of unit B3 still needs to be constrained, the most plausible attribution of the overlying glacial unit G2 is to MIS 4 possibly extending to early MIS 3. This stratigraphic position makes unit G2 roughly contemporaneous with the Middle Weichselian Eurasian glaciation (Barents–Kara Ice Sheet) constrained to between 50 and 60 ka [56], although glacial chronology for Eastern Siberia yet remains to be investigated.

A yet younger advance of a coherent ice mass on the East Siberian margin has been identified from a glaciogenic sedimentary wedge extending to ~ 650 mbpsl associated with a set of closely spaced recessional moraines [5]. Cores ARA03B-27 and ARA06C-03JPC, taken in front of this wedge, end in an extended grey unit below B2 (Figs. 1, 6, 7), suggesting that this event was older than ~ 45 ka, and could be a last re-advance of the major Middle Weichselian glaciation in this area.

The youngest glacial event affecting the East Siberian and Chukchi continental margin is indicated by numerous, densely spaced iceberg ploughmarks at ~ 150–350 mbpsl [2, 4–6, 57, 58]. The provenance of these icebergs, which may have had multiple sources, is not well-understood. As extensive iceberg ploughing obliterates earlier bedforms that may have existed in these seafloor areas, the presence of grounded coherent ice during MIS 2 (Late Weichselian) remains a contentious issue. The only evidence of MIS 2 ice-sheet grounding was provided for the eastern Chukchi margin (ramp to the Northwind Ridge) at water depths to ~ 420 m [1]. At any rate, the distribution of ice sheets at the East Siberian margin could not extend beyond the ploughmark belt. A very limited, if any, MIS 2 glaciation in this region is consistent with terrestrial studies from adjacent islands and mainland indicating ice-free conditions during the LGM [59–62]. We note, however, that glaciogenic sedimentary inputs during MIS 2 are indicated by the consistent presence of grey unit G1 in cores across the study area. More investigation is needed to better constrain its age and understand related depositional controls and provenance.

The stratigraphy of glacial events older than Middle Weichselian, indicated by multiple sets of glaciogenic bedforms at the East Siberian margin [5, 7], is poorly understood as cores retrieved on top of or close to these bedforms do not fully penetrate the sedimentary drape. Based on geophysical and sediment core data from the Lomonosov Ridge, the deepest ice grounding, identified at water depths reaching ~ 1200 mbpsl and thus assumed to be the thickest ice shelf covering the central Arctic Ocean, has been attributed to the penultimate major glaciation (MIS 6, ~ 140 ka) [4, 7, 17]. This age was also assigned to the last grounded ice event identified at the East Siberian margin in a sediment core recovered during the 2014 SWERUS Expedition close to the Arliss Plateau (core SWERUS-L2-13-PC1, 1119 mbpsl) [7]. A similar age interpretation was then proposed for SWERUS cores recovered in vicinity of glaciogenic landforms in the newly described De Long Trough at the East Siberian margin further northwest [8]. The age assignment in core SWERUS-L2-13-PC1, however, is based solely on a rare occurrence of calcareous nannofossils *Emiliana huxleyi* and *Gephyrocapsa* spp. in one sample from the second dark brown unit, attributed to MIS 5 [7]. While nannofossil records in the Arctic Ocean are generally interpreted in terms of the North Atlantic influence, with more abundant and diverse assemblages during major interglacials (such as MIS 7, 5 and 1) [50], coccoliths including *E. huxleyi* are also present in the intermediate stages, such as MIS 3 [50, 63], which complicates the age interpretation. The second brown unit in core SWERUS-L2-13-PC1 can be lithostratigraphically identified as unit B2 [64] that is well-constrained in multiple cores across the western Arctic Ocean, including the Arliss Plateau area, to MIS 3 as discussed above and illustrated in this study (Figs. 2, 4, 5, 6, 7). This stratigraphy constrains the last ice-grounding event off the East Siberian margin to the Middle Weichselian glaciation (MIS3/4). Both cores recovered from the De Long Trough (SWERUS-L2-23-GC1 and 24GC-1) contain a dark, poorly sorted, coarser grained basal sediment sequence interpreted as a glacial diamicton, which, in combination with the identified grounding zone deposit is interpreted as the last glacial advance in that area of the East Siberian margin [8]. O'Regan et al. [8] argue for an MIS 6 age of this last ice grounding in the De Long Trough in relation to evidence for MIS 6 ice scouring on the Lomonosov Ridge [7, 65], but also acknowledge a possible MIS 4 age for the recovered diamicton. Radiocarbon dates for sediments above the diamicton show ages of 33,200 ± 560 (SWERUS-L2-23-GC1) and 43,000 ± 1800 ^{14}C years BP (SWERUS-L2-24-GC1), which corroborate a Middle Weichselian age (MIS 3/4) for the last ice grounding in this area, consistent with the sediment stratigraphy in cores off the East Siberian and Chukchi margin presented in this study. The relationship of this glacial event with the broader Arctic glacial history, including the deepest erosion on the Lomonosov Ridge estimated as MIS 6 [4, 7], yet needs to be investigated.

Older glacial advances represented by yellowish-grey units below B3 have a more limited characterization in cores recovered in the study area, especially near the East Siberian margin due to an expanded unit G2 (Figs. 4, 5, 6, 7). Based on geophysical data [5], this glacial event, likely related to the Middle Weichselian glaciation, probably overprinted earlier depositional history in water depths to ~ 900 mbpsl along the margin. Cores further away from the margin display a series of grey/yellowish units potentially indicating glacial advances during MIS 5 stadials and MIS 6. The two better characterized grey units between B3 and B5, estimated as late MIS 5 stadials, increase in thickness towards the margin indicating it as a major sediment source similar to younger glacial events (Figs. 4, 5, 6, 7, 8). The glaciogenic nature of the grey unit below B4 is supported by its correlation to an over-consolidated diamicton with pre-glacial bedrock material in core PS72/342-1 (Figs. 6, 7) [13].

Summary and conclusions

The stratigraphic framework presented here is based on a combination of visual lithostratigraphy, physical properties, L^*, and Mn and Ca contents in sediment cores off the East Siberian and Chukchi margins of the western Arctic Ocean. The resulting core-to-core correlation is consistent within the study area, thus highlighting the stratigraphic potential of this approach.

Based on the developed correlation, stratigraphic recovery of cores along the W–E trending transect A from the East Siberian margin towards the Chukchi Borderland, extended to brown unit B5–B8 estimated as MIS 5c–7. In comparison, most cores from transect B stretching S–N along the Mendeleev Ridge towards a more southeastern part of the Siberian margin recovered a shorter stratigraphy ending in an extended grey unit G2 estimated to correspond to the Middle Weichselian glaciation (MIS 3/4). Overall, derived sedimentation rates show a decrease from the East Siberian/Chukchi shelves towards the central Arctic Ocean (Fig. 8), reflecting increasing distance from major sediment sources, longer residence times of material in the Beaufort Gyre circulation, and increased sea-ice cover.

The improved stratigraphic correlation aids better constraining the ages of glacial grounding events off the East Siberian margin. In particular, it suggests that the last major glacial advance into the Arctic Ocean in this area, with ice-sheet/-shelf grounding at depths to 850 mbpsl on the Arliss Plateau, was roughly contemporaneous with the Middle Weichselian glaciation in northern Eurasia, constrained in the Barents–Kara region to ca. 50–60 ka [56]. The presence of a younger, Late Weichselian ice sheet at the East Siberian margin is questionable. More studies are needed to clarify, whether such an ice sheet could have existed with a limited distribution at relatively shallow water depths (shallower than ~ 350 m) covered by intense iceberg scouring. Ice grounding during some of the older, pre-Mid-Weichselian advances extended to water depths as large as ~ 1200 mbpsl, as evidenced by older generations of MSGL at the Arliss Plateau [5]. Constraining the stratigraphy of these events is critical for reconstructing glacial history of the Arctic Ocean and northeastern Eurasia. In particular, reconciling glacial stratigraphies at the East Siberian and Chukchi margins with other glacially impacted Arctic seafloor areas, such as the Lomonosov Ridge, is much needed for understanding the timing and patterns of ice-sheet advances and ice-shelf formation in the Arctic Ocean.

Acknowledgements We would like to thank the captain and crew of RV Araon and RV Polarstern for excellent collaboration and support during expeditions ARA03B, ARA06B, and PS72. Work on this paper was funded by the Seed-type Research Program (no. PE18350) of the Korea Polar Research Institute. LP was supported by the US National Science Foundation awards ARC-0806999 and ARC-1304755. In addition, this paper is a contribution to the AWI Research Program PACES II, 3.1 and 3.2. Comments from two anonymous reviewers helped improving this manuscript.

Compliance with ethical standards

Conflict of interest On behalf of all authors, the corresponding author states that there is no conflict of interest.

References

1. Polyak L, Edwards MH, Coakley BJ, Jakobsson M (2001) Ice shelves in the Pleistocene Arctic Ocean inferred from glaciogenic deep-sea bedforms. Nature 410:453
2. Polyak L, Darby DA, Bischof JF, Jakobsson M (2007) Stratigraphic constraints on late Pleistocene glacial erosion and deglaciation of the Chukchi margin, Arctic Ocean. Quat Res 67:234–245
3. Jakobsson M, Polyak L, Edwards M, Kleman J, Coakley B (2008) Glacial geomorphology of the Central Arctic Ocean: the Chukchi Borderland and the Lomonosov Ridge. Earth Surf Proc Land 33:526–545
4. Jakobsson M, Nilsson J, O'Regan M, Backman J, Löwemark L, Dowdeswell JA, Mayer L, Polyak L, Colleoni F, Anderson LG, Björk G, Darby D, Eriksson B, Hanslik D, Hell B, Marcussen C, Sellén E, Wallin Å (2010) An Arctic Ocean ice shelf during MIS 6 constrained by new geophysical and geological data. Quat Sci Rev 29:3505–3517
5. Niessen F, Hong JK, Hegewald A, Matthiessen J, Stein R, Kim H, Kim S, Jensen L, Jokat W, Nam S-I, Kang S-H (2013) Repeated Pleistocene glaciation of the East Siberian continental margin. Nat Geosci 6:842–846
6. Dove D, Polyak L, Coakley B (2014) Widespread, multi-source glacial erosion on the Chukchi margin, Arctic Ocean. Quat Sci Rev 92:112–122
7. Jakobsson M, Nilsson J, Anderson L, Backman J, Bjork G, Cronin TM, Kirchner N, Koshurnikov A, Mayer L, Noormets R, O'Regan M, Stranne C, Ananiev R, Barrientos Macho N, Cherniykh D, Coxall H, Eriksson B, Floden T, Gemery L, Gustafsson O, Jerram K, Johansson C, Khortov A, Mohammad R, Semiletov I (2016) Evidence for an ice shelf covering the central Arctic Ocean during the penultimate glaciation. Nat Commun 7:1–13
8. O'Regan M, Backman J, Barrientos N, Cronin TM, Gemery L, Kirchner N, Mayer LA, Nilsson J, Noormets R, Pearce C, Semiletov I, Stranne C, Jakobsson M (2017) The De Long Trough: a newly discovered glacial trough on the East Siberian continental margin. Clim Past 13:1269–1284
9. Polyak L, Bischof J, Ortiz JD, Darby DA, Channell JET, Xuan C, Kaufman DS, Løvlie R, Schneider DA, Eberl DD, Adler RE, Council EA (2009) Late Quaternary stratigraphy and sedimentation patterns in the western Arctic Ocean. Glob Planet Change 68:5–17
10. Backman J, Jakobsson M, Løvlie R, Polyak L, Febo LA (2004) Is the central Arctic Ocean a sediment starved basin? Quat Sci Rev 23:1435–1454
11. Darby DA, Bischof JF, Jones GA (1997) Radiocarbon chronology of depositional regimes in the western Arctic Ocean. Deep Sea Res Part II 44:174–1757
12. Polyak L, Curry WB, Darby DA, Bischof J, Cronin TM (2004) Contrasting glacial/interglacial regimes in the western Arctic Ocean as exemplified by a sedimentary record from the Mendeleev Ridge. Palaeogeogr Palaeoclimatol Palaeoecol 203:73–93
13. Stein R, Matthiessen J, Niessen F, Krylov A, Nam S, Bazhenova E (2010) Towards a better (litho-) stratigraphy and reconstruction of Quaternary paleoenvironment in the Amerasian Basin (Arctic Ocean). Polarforschung 79:97–121
14. Nowaczyk NR, Frederichs TW, Eisenhauer A, Gard G (1994) Magnetostratigraphic data from late Quaternary sediments from the Yermak Plateau, Arctic Ocean: evidence for four geomagnetic polarity events within the last 170 ka of the Brunhes Chron. Geophys J Int 117:453–471
15. Nowaczyk NR, Antonow M, Knies J, Spielhagen RF (2003) Further rock magnetic and chronostratigraphic results on reversal excursions during the last 50 ka as derived from northern high latitudes and discrepancies in precise AMS14C dating. Geophys J Int 155:1065–1080
16. Jakobsson M, Løvlie R, Al-Hanbali H, Arnold E, Backman J, Mörth M (2000) Manganese and color cycles in Arctic Ocean sediments constrain Pleistocene chronology. Geology 28:23–26
17. Jakobsson M, Løvlie R, Arnold EM, Backman J, Polyak L, Knutsen JO, Musatov E (2001) Pleistocene stratigraphy and paleoenvironmental variation from Lomonosov Ridge sediments, central Arctic Ocean. Glob Planet Change 31:1–22
18. Jakobsson M, Backman J, Murray A, Løvlie R (2003) Optically stimulated luminescence dating supports central Arctic Ocean cm-scale sedimentation rates. Geochem Geophys Geosyst 4:1–11
19. Spielhagen RF, Baumann K-H, Erlenkeuser H, Nowaczyk NR, Nørgaard-Pedersen N, Vogt C, Weiel D (2004) Arctic Ocean deep-sea record of northern Eurasian ice sheet history. Quat Sci Rev 23:1455–1483
20. Channell JET, Xuan C (2009) Self-reversal and apparent magnetic excursions in Arctic sediments. Earth Planet Sci Lett 284:124–131
21. Xuan C, Channell JET, Polyak L, Darby DA (2012) Paleomagnetism of Quaternary sediments from Lomonosov Ridge and Yermak Plateau: implications for age models in the Arctic Ocean. Quat Sci Rev 32:48–63
22. Cronin TM, DeNinno LH, Polyak L, Caverly EK, Poore RZ, Brenner A, Rodriguez-Lazaro J, Marzen RE (2014) Quaternary

ostracode and foraminiferal biostratigraphy and paleoceanography in the western Arctic Ocean. Mar Micropaleontol 111:118–133
23. Matthiessen J, Schreck M, De Schepper S, Zorzi C, de Vernal A (2018) Quaternary dinoflagellate cysts in the Arctic Ocean: potential and limitations for stratigraphy and paleoenvironmental reconstructions. Quat Sci Rev 191:1–26
24. Brennan CE, Meissner KJ, Eby M, Hillaire-Marcel C, Weaver AJ (2013) Impact of sea ice variability on the oxygen isotope content of seawater under glacial and interglacial conditions. Paleoceanography 28:388–400
25. Alexanderson H, Backman J, Cronin TM, Funder S, Ingólfsson Ó, Jakobsson M, Landvik JY, Löwemark L, Mangerud J, März C, Möller P, O'Regan M, Spielhagen RF (2014) An Arctic perspective on dating Mid-Late Pleistocene environmental history. Quat Sci Rev 92:9–31
26. Clark DL, Whitman RR, Morgan KA, Mackey SD (1980) Stratigraphy and glacial—marine sediments of the Amerasian Basin, central Arctic Ocean. The Geological Society of America, Boulder, pp 1–57 **(special paper)**
27. Matthiessen J, Niessen F, Stein R, Naafs BDA (2010) Pleistocene glacial marine sedimentary environments at the eastern Mendeleev Ridge, Arctic Ocean. Polarforschung 79:123–137
28. Sellén E, O'Regan M, Jakobsson M (2010) Spatial and temporal Arctic Ocean depositional regimes: a key to the evolution of ice drift and current patterns. Quat Sci Rev 29:3644–3664
29. Bischof J, Clark DL, Vincent J-S (1996) Origin of ice-rafted debris: Pleistocene paleoceanography in the western Arctic Ocean. Paleoceanography 11:743–756
30. Phillips RL, Grantz A (1997) Quaternary history of sea ice and paleoclimate in the Amerasia basin, Arctic Ocean, as recorded in the cyclical strata of the Northwind Ridge. Geol Soc Am Bull 109:1101–1115
31. Phillips RL, Grantz A (2001) Regional variations in provenance and abundance of ice-rafted clasts in Arctic Ocean sediments: implications for the configuration of late Quaternary oceanic and atmospheric circulation in the Arctic. Mar Geol 172:91–115
32. Bazhenova E, Fagel N, Stein R (2017) North American origin of "pink-white" layers at the Mendeleev Ridge (Arctic Ocean): new insights from lead and neodymium isotope composition of detrital sediment component. Mar Geol 386:44–55
33. Polyak L, Jakobsson M (2011) Quaternary sedimentation in the Arctic Ocean: recent advances and further challenges. Oceanography 24:52–64
34. Adler RE, Polyak L, Ortiz JD, Kaufman DS, Channell JET, Xuan C, Grottoli AG, Sellén E, Crawford KA (2009) Sediment record from the western Arctic Ocean with an improved Late Quaternary age resolution: HOTRAX core HLY0503-8JPC, Mendeleev Ridge. Glob Planet Change 68:18–29
35. März C, Stratmann A, Matthiessen J, Meinhardt AK, Eckert S, Schnetger B, Vogt C, Stein R, Brumsack HJ (2011) Manganese-rich brown layers in Arctic Ocean sediments: Composition, formation mechanisms, and diagenetic overprint. Geochim Cosmochim Acta 75:7668–7687
36. Löwemark L, März C, O'Regan M, Gyllencreutz R (2014) Arctic Ocean Mn-stratigraphy: genesis, synthesis and inter-basin correlation. Quat Sci Rev 92:97–111
37. Wang R, Polyak L, Xiao W, Wu L, Zhang T, Sun Y, Xu X (2018) Late-Middle Quaternary lithostratigraphy and sedimentation patterns on the Alpha Ridge, central Arctic Ocean: implications for Arctic climate variability on orbital time scales. Quat Sci Rev 181:93–108
38. Meinhardt AK, März C, Schuth S, Lettmann KA, Schnetger B, Wolff JO, Brumsack HJ (2016) Diagenetic regimes in Arctic Ocean sediments: Implications for sediment geochemistry and core correlation. Geochim Cosmochim Acta 188:125–146
39. Wang R, Xiao W, März C, Li Q (2013) Late Quaternary paleoenvironmental changes revealed by multi-proxy records from the Chukchi Abyssal Plain, western Arctic Ocean. Glob Planet Change 108:100–118
40. Yurco LN, Ortiz JD, Polyak L, Darby DA, Crawford KA (2010) Clay mineral cycles identified by diffuse spectral reflectance in Quaternary sediments from the Northwind Ridge: implications for glacial–interglacial sedimentation patterns in the Arctic Ocean. Polar Res 29:176–197
41. Jokat W (ed) (2009) The Expedition of the Research Vessel "Polarstern" to the Arctic in 2008 (ARKXXIII/3). Berichte zur Polarforschung 597
42. Kang S-H, Nam S-I, Yim J-H, Chung K-H, Hong J-K (eds) (2012) Cruise report: RV Araon ARA03B, August 1–September 10, 2012, Chukchi Borderland and Mendeleyev Ridge
43. Best AI, Gunn DE (1999) Calibration of marine sediment core loggers for quantitative acoustic impedance studies. Mar Geol 160:137–146
44. Löwermark L, Chen H-F, Yang T-N, Kylander M, Yu E-F, Hsu Y-W, Lee T-Q, Song S-R, Jarvis S (2011) Normalizing XRF-scanner data: a cautionary note on the interpretation of high resolution records from organic-rich lakes. J Asian Earth Sci 40:1250–1256
45. Tjallingii R, Röhl U, Kölling M, Bickert T (2007) Influence of the water content on X-ray fluorescence core-scanning measurements in soft marine sediments. Geochem Geophys Geosyst 8:1–12
46. Jang K, Han Y, Huh Y, Nam S-I, Stein R, Mackensen A, Matthiessen J (2013) Glacial freshwater discharge events recorded by authigenic neodymium isotopes in sediments from the Mendeleev Ridge, western Arctic Ocean. Earth Planet Sci Lett 369:148–157
47. Poore RZ, Osterman L, Curry WB, Phillips RL (1999) Late Pleistocene and Holocene meltwater events in the western Arctic Ocean. Geology 27:759–762
48. O'Regan M, King J, Backman J, Jakobsson M, Pälike H, Moran K, Heil C, Sakamoto T, Cronin TM, Jordan RW (2008) Constraints on the Pleistocene chronology of sediments from the Lomonosov Ridge. Paleoceanography 23:PA1S19
49. Kaufman DS, Polyak L, Adler R, Channell JET, Xuan C (2008) Dating late Quaternary planktonic foraminifer *Neogloboquadrina pachyderma* from the Arctic Ocean using amino acid racemization. Paleoceanography 23:PA3224
50. Backman J, Fornaciari E, Rio D (2009) Biochronology and paleoceanography of late Pleistocene and Holocene calcareous nannofossil abundances across the Arctic Basin. Mar Micropaleontol 72:86–98
51. Comiso JC, Parkinson CL, Gersten R, Stock L (2008) Accelerated decline in the Arctic sea ice cover. Geophys Res Lett 35:L01703
52. Proshutinsky A, Bourke RH, McLaughlin FA (2002) The role of the Beaufort Gyre in Arctic climate variability: Seasonal to decadal climate scales. Geophys Res Lett 29:2100
53. Knies J, Vogt C (2003) Freshwater pulses in the Eastern Arctic Ocean during Saalian and Early Weichselian ice-sheet collapse. Quat Res 60:243–251
54. Bischof JF, Darby DA (1997) Mid- to Late Pleistocene ice drift in the western Arctic Ocean: evidence for a different circulation in the past. Science 277:74–78
55. Rudels B, Anderson L, Eriksson P, Fahrbach E, Jakobsson M, Melling EPJ, Prinsenberg H, Schauer S, Yao UT (2012) Observations in the Ocean. In: Lemke P (ed) Arctic climate change: the ACSYS decade and beyond. Springer, Berlin, pp 117–198
56. Svendsen JI, Alexanderson H, Astakhov VI, Demidov I, Dowdeswell JA, Funder S, Gataullin V, Henriksena M, Hjort C, Houmark-Nielsen M, Hubberten HW, Olfsson I, Jakobsson M, Kjæri KH, Larsen E, Lokrantz H, Pekka Lunkka J, Lyså A, Mangeruda J, Matiouchkov A, Murray A, Möller P, Niessen F, Nikolskaya O, Polyak L, Saarnisto M, Siegert M, Spielhagen RF, Stein R (2004)

Late Quaternary ice sheet history of northern Eurasia. Quat Sci Rev 23:1229–1271
57. Hill JC, Driscoll NW (2010) Iceberg discharge to the Chukchi shelf during the Younger Dryas. Quat Res 74:57–62
58. Gusev EA, Zinchenko AG, Bondarenko CA, Anikin NY, Derevjanko LG, Maksimov FE, Kuznetsov VY, Levchenko SB, Zherebtsov IE, Popov VV (2012) New data on the topography and Quaternary deposits of the outer shelf, East Siberian Sea. Geology and Geoecology of the Eurazian Continental Margin. GEOS, Moscow
59. Romanovskii N, Hubberten H-W, Gavrilov A, Tumskoy V, Kholodov AL (2004) Permafrost of the east Siberian Arctic shelf and coastal lowlands. Quat Sci Rev 23:1359–1369
60. Gualtieri L, Vartanyan SL, Brigham-Grette J, Anderson PM (2005) Evidence for an ice-free Wrangel Island, northeast Siberia during the last glacial maximum. Boreas 34:264–273
61. Stauch G, Gualtieri L (2008) Late Quaternary glaciations in northeastern Russia. J Quat Sci 23:545–558
62. Nikolsky DJ, Romanovsky VE, Romanovskii NN, Kholodov AL, Shakhova NE, Semiletov IP (2012) Modelling sub-sea permafrost in the East Siberian Arctic Shelf: the Laptev Sea region. J Geophys Res Earth Surf 117:F03028
63. Gard G, Backman J (1990) Synthesis of Arctic and Subarctic coccolith biochronology and history of North Atlantic drift water influx during the last 500.000 years. In: Bleil U, Thiede J (eds) Geological history of the Polar Oceans: Arctic versus Antarctic. Kluwer, Dordrecht, pp 417–436
64. The SWERUS Scientific Party (2016) Cruise report SWERUS-C3 Leg 2. Meddelanden från Stockholms universitets Bolin Centre for Climate Research No. 2
65. Stein R, Fahl K, Gierz P, Niessen F, Lohmann G (2017) Arctic Ocean sea ice cover during the penultimate glacial and the last interglacial. Nat Commun 8:373
66. Jakobsson M, Mayer LA, Coakley B, Dowdeswell JA, Forbes S, Fridman B, Hodnesdal H, Noormets R, Pedersen R, Rebesco M, Schenke H-W, Zarayskaya AY, Accettella D, Armstrong A, Anderson RM, Bienhoff P, Camerlenghi A, Church I, Edwards M, Gardner JV, Hall JK, Hell B, Hestvik OB, Kristoffersen Y, Marcussen C, Mohammad R, Mosher D, Nghiem SV, Pedrosa MT, Travaglini PG, Weatherall P (2012) The international bathymetric chart of the Arctic Ocean (IBCAO) version 3.0, Geophys Res Lett. https://doi.org/10.1029/2012GL052219
67. Jakobsson M, Andreassen K, Bjarnadóttir LR, Dove D, Dowdeswell JA, England JH, Funder S, Hogan K, Ingólfsson Ó, Jennings A, Krog Larsen N, Kirchner N, Landvik JY, Mayer L, Mikkelsen N, Möller P, Niessen F, Nilsson J, O'Regan M, Polyak L, Nørgaard-Pedersen N, Stein R (2014) Arctic Ocean glacial history. Quat Sci Rev 92:40–67